Wavepacket Splitting and Two-Pathway Deactivation in the Photoexcited Visual Pigment Isorhodopsin**

Dario Polli, Oliver Weingart, Daniele Brida, Emiliano Poli, Margherita Maiuri, Katelyn M. Spillane, Andrea Bottoni, Philipp Kukura, Richard A. Mathies, Giulio Cerullo, and Marco Garavelli**

The protonated Schiff base of 11-*cis* retinal (PSB11) is the chromophore of the visual pigment Rhodopsin (Rh).[1,2] The transduction activity of Rh is triggered by an ultrafast (200 fs)[3–7] and highly efficient (0.65 quantum yield, QY)[8] light-induced *cis–trans* isomerization of PSB11[9,10] to form the primary photoproduct photorhodopsin (photoRh). This process can be described as the ballistic motion of a photoexcited wavepacket from the Franck–Condon (FC) region through a conical intersection (CI) between ground and excited states. The speed and efficiency of the photoisomerization in the visual pigment depend upon two key parameters: 1) The protein pocket. In solution, the QY is smaller and the photoisomerization is almost two orders of magnitude slower;[11] and 2) the specific configuration of the chromophore within the protein pocket. In the case of isorhodopsin (isoRh), where 9-*cis*-retinal (PSB9) is embedded in the same opsin environment, the 9-*cis*→all-*trans* photoisomerization reaction is three times slower (600 fs)[12] and is less effective at triggering a visual response (0.22 QY).[13] As first reported by Yoshizawa and Wald,[9] photoisomerization of isoRh results in the production of the same batho-rhodopsin (bathoRh) intermediate as for Rh. In fact, Rh, bathoRh and isoRh form, upon irradiation, a steady-state three-component photoequilibrium.[10,14] The longer isomerization time and smaller quantum yield in isoRh were assigned to a lower wavepacket speed along the torsional isomerization coordinate.[12]

Herein, we employ a combined experimental/computational approach to provide the mechanistic rationale behind the less-efficient PSB9 photoisomerization and the delayed photoRh formation. Ultrafast optical spectroscopy with sub-20 fs time resolution and spectral coverage extended to the near-infrared (NIR) allows us to track wavepacket motion from the photoexcited FC region to the photoproduct by directly probing the reactant excited state dynamics through its stimulated emission (SE). The mechanistic scenario unraveled by quantum-mechanical (QM)/molecular-mechanical (MM) molecular dynamics (MD), which accounts for the recorded features in SE decay and timescale, challenges the

[*] Dr. D. Polli, Dr. D. Brida, M. Maiuri, Prof. G. Cerullo
IFN-CNR, Dipartimento di Fisica, Politecnico di Milano
Piazza L. da Vinci, 32, 20133 Milano (Italy)
E-mail: giulio.cerullo@fisi.polimi.it
E. Poli, Prof. A. Bottoni, Dr. M. Garavelli
Dipartimento di Chimica "G. Ciamician" Università di Bologna
Via F. Selmi 2, 40126 Bologna (Italy)
E-mail: marco.garavelli@unibo.it
Dr. O. Weingart
Institut für Theoretische Chemie und Computerchemie
Heinrich-Heine-Universität Düsseldorf
Universitätsstrasse 1, 40225 Düsseldorf (Germany)
Dr. K. M. Spillane, Dr. P. Kukura
Department of Chemistry, University of Oxford
Oxford OX1 3QZ (UK)
Prof. R. A. Mathies
Chemistry Department, University of California at Berkeley
Berkeley, CA 94720 (USA)
Dr. D. Polli
Center for Nano Science and Technology @Polimi
Italian Institute of Technology
Via G. Pascoli 70/3, 20133 Milano (Italy)
Dr. M. Garavelli
Laboratoire de Chimie, LR6, Ecole Normale Supérieure de Lyon
46, allée d'Italie, 69364 Lyon, cedex 07 (France)
Dr. D. Brida
Department of Physics, University of Konstanz
78457 Konstanz (Germany)
E. Poli
Department of Chemistry, University of Liverpool
Oxford Street, Liverpool L69 3BX (UK)

[**] G.C. and M.G. acknowledge support by the European Research

currently accepted view of a single and slower decay path in isoRh photochemistry. Indeed, we find that the reaction path rapidly branches towards two competitive deactivation channels involving a backward and forward bicycle pedal motion of the C9=C10 and C11=C12 double bonds, respectively. These pathways lead to two different CI funnels: one is rapidly accessed, but unreactive; the other is accessed later and produces bathoRh after excited state decay. This wavepacket splitting and the different decay rates are responsible for the reduced QY and the slower isomerization that is observed in isoRh as compared to Rh. The spectroscopic signatures arising from these individual pathways add together and explain the strongly non-exponential decay observed in the SE.

The isoRh sample is generated by illuminating Rh, prepared by isolating rod outer segments from bovine retinas,[15] with laser radiation at 568 nm for 30 min at 77 K. We initiated the photoisomerization by a 10 fs pump pulse centered at 500 nm in resonance with the ground-state isoRh absorption, and probed the differential transmission ($\Delta T/T$) signal using both sub-10 fs visible (500–680 nm) and 13 fs NIR pulses (840–1020 nm). The experimental setup is described in detail in the Supporting Information and in Ref. [16]. The time resolution was better than 20 fs over the entire spectral range. The sample was flowed to ensure complete replacement in the focal volume for each consecutive laser shot.

Our $\Delta T/T$ data in the visible (see the Supporting Information) are in excellent agreement with previous results by Schoenlein et al.,[12] and show the build-up of the photoRh photoproduct, with photoinduced absorption (PA) red-shifted with respect to the ground-state absorption of the reactant.[17] However, in the visible spectral region, the signal is the result of several overlapping contributions:[12] an initial PA from the excited state of the PSB9 reactant, which rises upon pump excitation, a subsequent PA from the hot ground state of the non-isomerized reactant (produced with ca. 80 % efficiency), and finally the PA from the isomerized all-*trans* photoproduct. This strong overlap makes it cumbersome to directly extract isoRh dynamics. On the other hand, the novel NIR spectral window directly probes the excited state of the reactant via its SE, as previously shown for the case of Rh.[18] Figure 1 a presents the 2D $\Delta T/T$ map in the NIR, as a function of probe wavelength and pump-probe delay. The signal features a prompt rise of the SE at short wavelengths (850 nm) that rapidly shifts to longer wavelengths because the energy gap between ground and excited states decreases as the wavepacket moves towards the CI.[18] The SE signal displays a strongly non-exponential decay, with an initial fast component completed within ca. 150 fs, followed by a weaker plateau that lasts until ca. 400 fs after the pump pulse (Figure 1 b). This two-component decay of the SE, which is radically different from the dynamics observed in Rh,[18] is not consistent with the picture of a single wavepacket which moves ballistically through a CI.

To extract a dynamic model of the photoinduced process, we simulated (through the COBRAMM interface)[19] the evolution of the opsin-embedded PSB9 chromophore from the excited to the ground electronic state by employing

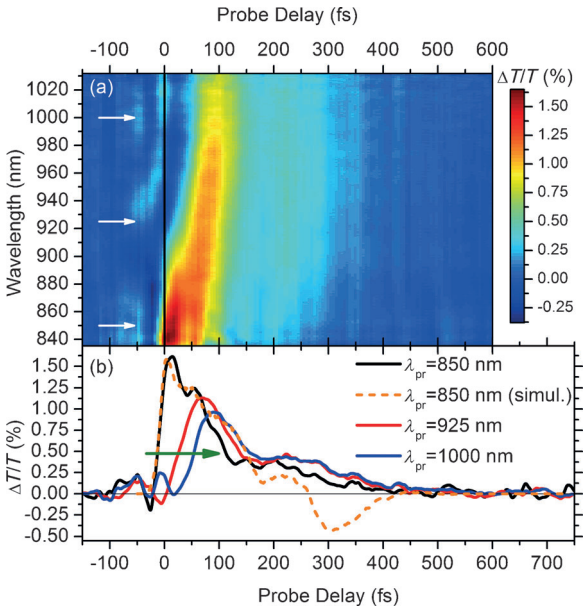

Figure 1. a) Differential transmission ($\Delta T/T$) map of isoRh in the NIR range, following excitation by a 10 fs pulse at 500 nm; b) solid lines: time traces at selected probe wavelengths; dashed line: MD-simulated trace at 850 nm. The green arrow indicates the delayed formation of the SE for longer wavelengths.

a statistically meaningful set of hybrid QM/MM trajectories. Similar methods have been previously used to track photo-induced dynamics in Rh[18–21] and other biomolecules.[22–25] We used a joined QM/MM approach employing ab initio complete active space-self consistent field (CASSCF(10/10)/6-31G*) with electrostatic and MM embedding wavefunction,[23] and the Amber99ff force field. This combination has proven to be an accurate method for quantitative studies in retinal proteins[18,24] (see also the Supporting Information). We simulated transient signals using scaled CASSCF transition energies,[18] thus approaching the accuracy of full non-adiabatic complete active space with second-order perturbation theory (CASPT2)[25] dynamics that are currently possible only for smaller systems.[26] All of the atoms are fixed at their crystallographic positions, except for the chromophore and a 5 Å-thick protein pocket region surrounding it. An ensemble of 81 initial conditions was generated by thermally sampling the vibrational modes at room temperature. We included zero-point energy corrections but excluded high-frequency C–H, N–H, and O–H modes. The details of the system set-up, QM model reduction and the dynamics are presented in the Supporting Information.

The computed trajectories for C9=C10 and C11=C12 twisting motion toward the different photoproducts are shown in Figure 2 a. The swarm of trajectories initially created in the PSB9 FC region branches within about 30 fs and almost equally populates two competitive radiationless decay routes. These distinct channels eventually lead to two very different CI funnels, named here $CI_1(++)$ and $CI_2(--)$. They are accessed by bicycle pedal motions along the two double bonds in reverse or forward directions (Figure 2 a). The different steric interactions with the protein environment lead to

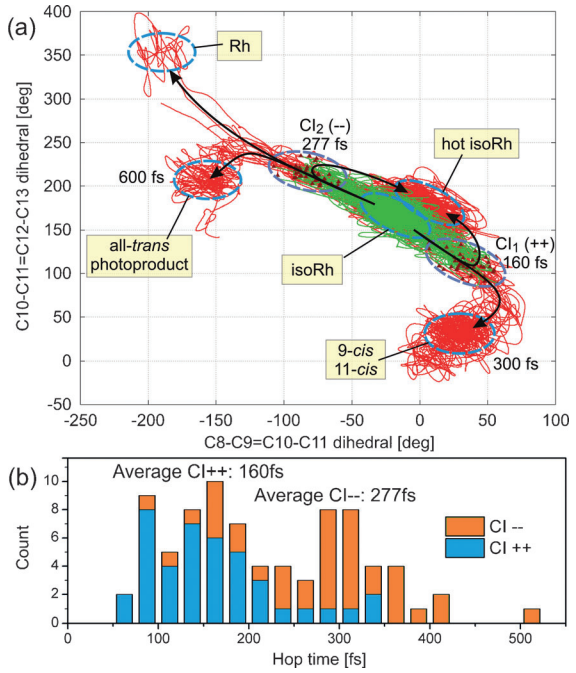

Figure 2. a) Overlay of the 81 computed isoRh trajectories from FC to the different molecular outcomes as a function of the C_9=C_{10} and the C_{11}=C_{12} dihedral twist with average reaction times and final configurations. The paths turn from green to red with the excited to ground state surface hop at one of the two CIs. b) Distribution of S_1 lifetimes with channels and average hop times.

different average access times, namely about 160 fs for $CI_1(++)$ and about 280 fs for $CI_2(--)$ (Figure 2b). Access to $CI(--)$ is delayed mainly due to interactions between H–C11 and TYR268 in the forward path, thus featuring an extended energy plateau, while counterclockwise motion of the H–C10–C11–H fragment can proceed without major hindrance and is thus faster (Figure 3a). The shapes of the reaction paths for the two channels are responsible for the experimentally observed non-exponential two-component decay of the SE signal (see the simulated $\Delta T/T$ dynamics as a dashed line in Figure 1b). Note that the simulation yields

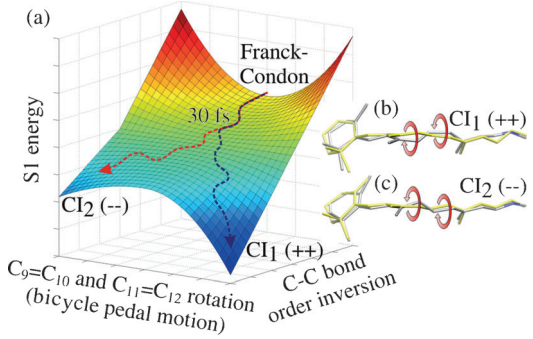

Figure 3. a) Model of isoRh S_1 potential energy surface along bicycle pedal motion and bond inversion coordinates. b, c) Averaged structures of the chromophore at the CI_1 and CI_2 configurations respectively (gray) compared with the FC configuration (yellow). The red arrows indicate the reverse/forward bicycle pedal motions.

a small PA signal after about 250 fs, which is not observed in the experiment. This discrepancy is a result of the limitations in simulation method and statistics and of the delicate balance between the contribution of different deactivation pathways in the $\Delta T/T$ signal of isoRh. Qualitatively similar results have been obtained in recent calculations on isoRh[27] performed at lower computational level (CAS(6,6)/6-31G), and neglecting electrostatic wavefunction polarization effects. The latter are important to account for the influence of the environment on the photochemically relevant S_1 charge transfer state and for the calculation of experimentally compatible transient spectroscopic data and energies. However, the existence of both decay channels in mechanical embedding calculations demonstrates that wavepacket splitting and population of the two competitive decay routes are caused by steric effects.

The two deactivation pathways can be further characterized by the direction of the bicycle pedal motion. Motion toward $CI_1(++)$ involves a positive twist along C9=C10 together with strong negative twist along C11=C12 (Figure 3b). This "reverse" pedal motion in the excited state is the same responsible for the rapid generation of photoRh[18,28] in Rh. In our calculations, isoRh molecules entering $CI_1(++)$ either revert back to the ground state of the reactant or undergo a strong twist along the C11=C12 dihedral, thus forming a di-*cis* photoproduct (9,11-di-*cis*; Figure 2a). Note that in both cases the C9=C10 photoisomerization is aborted. Only the slower channel involving decay through $CI_2(--)$ and forward pedal rotation (Figure 3c), that is, strong negative C9=C10 rotation and positive torsion at C11=C12, can generate the all-*trans* photoproduct with a quantum yield of 16% (±4%; see also the Supporting Information). This value is in good agreement with experimental observation (22%) and the slower 600 fs all-*trans* photoproduct formation observed in isoRh compared to Rh.[12] Furthermore, we also observe three trajectories leading to a full bicycle pedal Rh-like photoproduct (9-*trans*-11-*cis*, Figure 2a).

The double-channel decay mechanism with population splitting has been also confirmed through both simulations without initial velocities, and more accurate but much more expensive full active space CAS(12,12)/MM computations on a subset of trajectories (see the Supporting Information). In the former set, the trajectories more closely follow the surface topology with less thermal fluctuations, providing an even better agreement with the experimental spectroscopic signal and a similar quantum yield (19±4%, see also Supporting Information). The CAS(12,12) calculations, although preventing a full statistical and spectroscopic analysis owing to their cost, suggest a smaller QY (<5%) for the 9,11-di-*cis* photoproduct, thus explaining the lack of experimental evidence to date for this product.

Despite sharing the same apoprotein environment, Rh and isoRh display a remarkably different photochemistry, which is caused by the different configuration of the retinal chromophore and its steric interactions. The photoreactions in both proteins are nevertheless triggered by a unique reaction coordinate, that is bicycle pedal motion along the C9=C10 and C11=C12 double bonds. In the protein pocket, 9-*cis* retinal operates in both forward and reverse bicycle pedal directions, while the forward path is blocked for 11-*cis* retinal.

In both compounds, the fast decay channel is associated with reverse bicycle pedal motion. In isoRh this deactivation path is non-productive; reaction toward photoRh proceeds only in the forward direction, featuring extended steric interactions with the protein environment and thus significantly slower reaction time (Figure 3). These results agree with the findings of Strambi et al.,[29] stating that Rh and isoRh share a common valley on the excited state potential energy surface, just starting from opposite ends (Figure 2a). The branching of the excited-state population into slower productive and faster unproductive channels explains the reduced activity and quantum yield in isoRh as compared to Rh, where only the fast and productive path is populated and a higher QY obtained. Thus the photoisomerisation in isoRh proceeds by a two-channel decay mechanism, while the direction of torsion in Rh is unique. These data call for isoRh as an ideal candidate for coherent control experiments,[30] as suppressing one or the other of the two decay channels would result in a drastically different photophysics and photochemistry than for the uncontrolled compound.

Received: November 13, 2013
Published online: January 31, 2014

[1] H. Kandori, Y. Shichida, T. Yoshizawa, *Biochemistry* **2001**, *66*, 1197 – 1209.
[2] R. A. Mathies, J. Lugtenburg in *Handbook of Biological Physics*, *Vol. 3* (Eds.: D. G. Stavenga, W. J. DeGrip, E. N. Pugh), Elsevier Science, Amsterdam, **2000**, pp. 55 – 90.
[3] R. W. Schoenlein, L. A. Peteanu, R. A. Mathies, C. V. Shank, *Science* **1991**, *254*, 412 – 415.
[4] G. Haran, E. A. Morlino, J. Matthes, R. H. Callender, R. M. Hochstrasser, *J. Phys. Chem. A* **1999**, *103*, 2202 – 2207.
[5] H. Chosrowjan, N. Mataga, Y. Shibata, S. Tachibanaki, H. Kandori, Y. Shichida, T. Okada, T. Kouyama, *J. Am. Chem. Soc.* **1998**, *120*, 9706 – 9707.
[6] H. Kandori, Y. Furutani, S. Nishimura, Y. Shichida, H. Chosrowjan, Y. Shibata, N. Mataga, *Chem. Phys. Lett.* **2001**, *334*, 271 – 276.
[7] G. G. Kochendoerfer, R. A. Mathies, *J. Phys. Chem.* **1996**, *100*, 14526 – 14532.
[8] J. E. Kim, M. J. Tauber, R. A. Mathies, *Biochemistry* **2001**, *40*, 13774 – 13778.
[9] T. Yoshizawa, G. Wald, *Nature* **1963**, *197*, 1279 – 1286.
[10] G. A. Schick, T. M. Cooper, R. A. Holloway, L. P. Murray, R. R. Birge, *Biochemistry* **1987**, *26*, 2556 – 2562.
[11] S. L. Logunov, L. Song, M. A. El Sayed, *J. Phys. Chem.* **1996**, *100*, 18586 – 18591.
[12] R. W. Schoenlein, L. A. Peteanu, Q. Wang, R. A. Mathies, C. V. Shank, *J. Phys. Chem.* **1993**, *97*, 12087 – 12092.
[13] J. B. Hurley, T. G. Ebrey, B. Honig, M. Ottolenghi, *Nature* **1977**, *270*, 540 – 542.
[14] S. J. Hug, J. W. Lewis, D. S. Kliger, *J. Am. Chem. Soc.* **1988**, *110*, 1998 – 1999.
[15] I. Palings, J. A. Pardoen, E. van den Berg, C. Winkel, J. Lugtenburg, R. A. Mathies, *Biochemistry* **1987**, *26*, 2544 – 2556.
[16] C. Manzoni, D. Polli, G. Cerullo, *Rev. Sci. Instrum.* **2006**, *77*, 023103.
[17] S. Hahn, G. Stock, *J. Phys. Chem. B* **2000**, *104*, 1146 – 1149.
[18] D. Polli, P. Altoe, O. Weingart, K. M. Spillane, C. Manzoni, D. Brida, G. Tomasello, G. Orlandi, P. Kukura, R. A. Mathies, M. Garavelli, G. Cerullo, *Nature* **2010**, *467*, 440 – 443.
[19] P. Altoè, M. Stenta, A. Bottoni, M. Garavelli, *Theor. Chem. Acc.* **2007**, *118*, 219 – 240.
[20] L. M. Frutos, T. Andruniow, F. Santoro, N. Ferre, M. Olivucci, *Proc. Natl. Acad. Sci. USA* **2007**, *104*, 7764 – 7769.
[21] S. Hayashi, E. Tajkhorshid, K. Schulten, *Biophys. J.* **2009**, *96*, 403 – 416.
[22] G. Groenhof, L. V. Schafer, M. Boggio-Pasqua, M. Goette, H. Grubmüller, M. A. Robb, *J. Am. Chem. Soc.* **2007**, *129*, 6812 – 6819; H. R. Hudock, B. G. Levine, A. L. Thompson, H. Satzger, D. Townsend, N. Gador, A. Stolow, T. J. Martinez, *J. Phys. Chem. A* **2007**, *111*, 8500 – 8508; H. R. Hudock, T. J. Martinez, *ChemPhysChem* **2008**, *9*, 2486 – 2490; S. Maeda, K. Morokuma, *J. Chem. Theory Comput.* **2011**, *7*, 2335 – 2345.
[23] M. Wanko, M. Hoffmann, P. Strodel, A. Koslowski, W. Thiel, F. Neese, T. Frauenheim, M. Elstner, *J. Phys. Chem. B* **2005**, *109*, 3606 – 3615.
[24] G. Tomasello, G. Olaso-González, P. Altoè, M. Stenta, L. Serrano-Andrés, M. Merchán, G. Orlandi, A. Bottoni, M. Garavelli, *J. Am. Chem. Soc.* **2009**, *131*, 5172 – 5186.
[25] K. Andersson, P.-A. Malmqvist, B. Roos, *J. Chem. Phys.* **1992**, *96*, 1218 – 1226.
[26] H. Tao, B. G. Levine, T. J. Martinez, *J. Phys. Chem. A* **2009**, *113*, 13656 – 13662.
[27] W. C. Chung, S. Nanbu, T. Ishida, *J. Phys. Chem. B* **2012**, *116*, 8009 – 8023.
[28] A. Warshel, *Nature* **1976**, *260*, 679 – 683.
[29] A. Strambi, P. B. Coto, L. M. Frutos, N. Ferré, M. Olivucci, *J. Am. Chem. Soc.* **2008**, *130*, 3382 – 3388.
[30] V. I. Prokhorenko, A. M. Nagy, S. A. Waschuk, L. S. Brown, R. R. Birge, R. J. D. Miller, *Science* **2006**, *313*, 1257 – 1261.